Illuminating Anions in Biology with Genetically Encoded Fluorescent Biosensors

Mariah A. Cook[†‡], Shelby M. Phelps[†‡], Jasmine N. Tutol[†‡], Derik A. Adams[†], and Sheel C. Dodani[†*]

[†]Department of Chemistry and Biochemistry, The University of Texas at Dallas, Richardson, TX 75080

[‡]M.A.C., S.M.P., and J.N.T. contributed equally to this work.

*E-mail: sheel.dodani@utdallas.edu

Abbreviations

Adenosine triphosphate (ATP), cyclic adenosine monophosphate (cAMP), cystic fibrosis transmembrane conductance regulator (CFTR), direct coupling analysis (DCA), days *in vitro* (DIV), endoplasmic reticulum (ER), *Escherichia coli* (*E. coli*), excitatory amino acid transporter 1 (EAAT1), fluorescence lifetime imaging microscopy (FLIM), fluorescent protein (FP), Förster resonance energy transfer (FRET), glucosamine (GlcN), green fluorescent protein from *Aequorea victoria* (avGFP), guanosine diphosphate (GDP), guanosine triphosphate (GTP), hydroxycarboxylic acid receptor 1 (HCAR1), local calcium release (LCR), multiple sequence alignment (MSA), signal-to-noise ratio (SNR), sinoatrial node pacemaker cells (SANPCs), site-saturation mutagenesis (SSM), solute binding protein (SBP), SuperClomeleon mouse model (SClm), two-photon (2P), uridine diphosphate *N*-acetylglucosamine (UDP-GlcNAc)

Introduction

The chemical composition of biological anions is diverse, ranging from monoatomic halides like chloride to polyatomic species like ATP [1]. Anion networks exist in extracellular, cytosolic, and subcellular pools over a wide concentration range (nM – mM) intricately coordinating essential processes, including regulation of cation flux for cell signaling and post-translational modifications for gene expression, metabolism, and

detoxification, among others (Figure 1a) [2–17]. To investigate the cellular recognition, membrane transport, and metabolic transformation of anions across these functions, researchers have historically relied on biochemical assays and physiological techniques [18–20]. As a complement, the development and use of genetically encoded fluorescent biosensors for live cell imaging has become a fundamental approach to monitor and measure the spatiotemporal dynamics of anions.

The advent of green fluorescent protein from the jellyfish *Aequorea victoria* (avGFP) has revolutionized the field of live cell imaging due to its tunable genetically encoded framework, biocompatibility, and targetability without the need for an exogenous chromophore (Figure 1b) [21,22]. Biosensors based on avGFP and its derivatives, either as standalone scaffolds or in fusion with naturally occurring anion binding proteins, have been applied for imaging labile anion pools in bacteria, plant, and mammalian cells (Figure 1c). While the development of FP biosensors has historically focused on cations, the field of anion FP biosensor development is booming and continues to expand at a rapid pace [23].

To inspire innovations in this field, we have structured this Review to be a guide for new toolmakers and end users, providing considerations that should be made in the selection, design, development, and application of FP biosensors for anions. Here, we have drawn focus to biologically relevant anions including chloride (Cl^-), oxyanions (i.e., nitrate, NO_3^-; phosphate, PO_4^{3-}; sulfate, SO_4^{2-}), carboxylates (i.e., D-aspartate, D-glutamate, L-lactate), and nucleotides (i.e., ATP, cAMP, GTP/GDP, UTP/UDP) (Table 1). Of the many advancements made over the last three years, we will highlight exemplary case studies that have uncovered unprecedented biological observations through clever strategies for biosensor (i) design, (ii) engineering, and (iii) imaging applications.

Biosensor Designs and Mechanisms

Intrinsic Biosensors

Single domain FPs with intrinsic anion binding pockets proximal to the chromophore can be sensitive to halides and oxyanions (Figure 1c). The pioneering discovery of avGFP

with a key tyrosine mutation at position 203 above the chromophore catalyzed the field of intrinsic biosensors for chloride more than twenty years ago [24,25]. This scaffold has since been exploited to generate a palette of biosensors with intensiometric and ratiometric fluorescence outputs [26]. Recently, new biosensors bearing the homologous tyrosine residue have been uncovered through genomic mining and rational design. Included are GFPxm163 from *Aequorea macrodactyla* and mBeRFP from *Entacmaea quadricolor*. The binding of chloride resulted in fluorescence quenching by tuning the chromophore pK_a in the case of GFPxm163, or static quenching in mBeRFP [27,28]. One noteworthy anion-sensitive scaffold is mNeonGreen with an arginine in place of the tyrosine above the chromophore. Mutagenesis near the binding pocket or protein chromophore unlocked a new turn-on sensing mechanism at physiological pH for chloride with the ChlorON series and enhanced binding kinetics for sulfate with SulfOFF-1, respectively [29,30]. Beyond the GFP family, the chloride biosensors GR1-CFP, GR2-CFP, and ChloRED-1-CFP have been engineered from membrane-bound, proton-pumping microbial rhodopsins, affording red-shifted excitation and emission profiles [31–33]. A single point mutation at the counterion position to the protonated Schiff-base chromophore created a chloride binding pocket. In these biosensors, chloride binding stabilized the protonated, fluorescent form of the chromophore generating a ratiometric, turn-on response across a wide pH range.

Extrinsic Biosensors

Anion recognition domains such as solute binding proteins (SBP), enzymes, transcription factors, and transporters, can be inserted into and between FP reporter domain(s) to generate extrinsic biosensors (Figure 1c). Stemming from the first single FP extrinsic biosensor camgaroo1, [34] recognition domains are typically inserted into a disordered region near the FP chromophore known as the β-bulge [35]. On the other hand, to create FRET-based biosensors, the recognition domain is often sandwiched between the termini of a donor and acceptor FP [36]. In either design, the anion binding event induces a conformational change in the recognition domain. This is then relayed to the chromophore(s) in the FP reporter(s), resulting in an intensiometric, ratiometric, FRET, or fluorescence lifetime response. For further reading into the designs and mechanisms of

extrinsic biosensors, we refer the interested reader to the reviews by Nasu et al. and Sanchez et al. [35,36]. The modularity of extrinsic biosensors is best exemplified by the recent boom of lactate biosensors: GEM-IL, eLACCO2.1, R-iLACCO2, iLACCO1, LARS1.8, LiLac, CanlonicSF, FiLLac$_{10N0C}$, FiLa (Table 1) [37–45]. The recognition domains used in these designs span the *Escherichia coli* periplasmic SBP TTHA0766, *E. coli* transcription factor LldR, *Heliobacter pylori* chemotaxis protein TlpC, and mouse hydroxycarboxylic acid receptor 1 (HCAR1). In combination with a variety of FP reporter domains and engineering strategies, these lactate biosensors have probed lactate metabolism across a range of biological applications.

Protein Engineering Strategies to Improve Biosensor Properties

Sequence and Structure-Guided Approaches

While traditional protein engineering techniques have stood the test of time, these can be enhanced by integrating computational modeling and structural studies [46,47]. In turn, enabling effective and focused sequence space exploration.

Examples of sequence-guided biosensor engineering include the lactate biosensor C-GEM-IL 3.0 and the chloride biosensor GR2-CFP [32,37]. Bekdash et al. engineered the GEM-IL series for lactate consists of fusions between the bacterial lactate recognition LldR domain and SuperFolder green (G-GEM-IL), yellow (Y-GEM-IL), and cyan (C-GEM-IL) FPs [37]. Multiple sequence alignment (MSA) between the GEM-IL series followed by the LldR domains from different organisms were used to identify consensus. In lieu of a crystal structure, homology modeling software including SWISS MODEL and I-TASSER provided further support [48,49]. Based on this analysis, mutagenesis of a single residue in both the FP and LldR domains enhanced the dynamic range and binding affinity for lactate.

MSAs can be further leveraged with the Direct Coupling Analysis (DCA) statistical model to extract how amino acids coevolve across a given protein family [50]. This approach was used to analyze the rhodopsin family and engineer GR1-CFP to GR2-CFP using iterative site-saturation mutagenesis (SSM) along five key residues in the proton-pumping

pathway (Figure 2a). The DCA model not only verified the functional connectivity between these residues, but also defined the mutational space and order. Thereby reducing the sampling needed to identify variants with improved dynamic range.

Further, structural information can inform engineering efforts. This point can be illustrated with the generation of the ChlorONs from mNeonGreen by Tutol et al [30,51]. Based on the crystal structures of mNeonGreen at pH 4.5 and pH 8, two non-coordinating residues near the chromophore were selected for combinatorial SSM (Figure 2b) [30,52,53]. A strategy termed anion walking, akin to substrate walking in biocatalysis, was developed to screen for sensitivity to bromide in *E. coli* lysate at pH 8 [54]. Bromide is spherical in shape like chloride but has a lower dehydration penalty, resulting in higher affinity complexes with FPs [51,55]. With this logic, bromide was used as a surrogate to screen ~2,000 variants and discover three standalone, turn-on fluorescent biosensors that can directly monitor endogenous chloride pools in a cell model overexpressing the cystic fibrosis transmembrane conductance regulator (CFTR) [30].

Promiscuous anion binding can also be observed and exploited in natural anion recognition domains. This has recently been demonstrated with the aspartate biosensor jAspSnFR3 engineered from a variant of the glutamate biosensor iGluSnFR [56]. The latter relies on the glutamate/aspartate GltI recognition domain, which binds glutamate with a higher affinity than aspartate. The crystal structure of GltI bound to glutamate was used to identify residues that could shift the selectivity towards aspartate. Specifically, two coordinating serine residues were subjected to iterative SSM, followed by expression in *E. coli*, and screening in lysate. The resulting jAspSnFR3 biosensor has a notable preference for aspartate over other biologically relevant metabolites, including glutamate and asparagine, enabling powerful quantitation of intracellular aspartate dynamics.

Application-driven Approaches

A mantra in protein engineering is, “You get what you screen for.” [57] This can be encountered when biosensor performance is compromised, particularly in unexplored applications [58]. While unsurprising, such observations should be heeded as a warning

to end users and motivation to toolmakers. To address this, protein engineering workflows have been modified such that biosensor screening and selection can be carried out with the cell model intended for study or even the instrumentation of choice. Demonstrations of these modifications include the glutamate biosensor iGluSnFR3 and lactate biosensor LiLac [42,59].

Most iGluSnFR variants suffer from low signal-to-noise ratios (SNR) and saturating activation kinetics to image glutamate dynamics *in vivo* [60]. To overcome this, a multi-system directed evolution workflow was developed by Aggarwal et al. [59] The parent SF-Venus-iGluSnFR-A184V was first subjected to twenty rounds of sequence diversification through SSM, random mutagenesis, and recombination libraries. Variants were first screened in *E. coli* for fluorescence (~10^5 variants per round), then in lysate for increased dynamic range (~400 variants per round), and finally in purified form for (i) glutamate affinity, (ii) 2P fluorescence, and (iii) kinetics (<20 variants per round). While screening in *E. coli* allows for rapid sampling of large libraries, it can also be limiting when biosensor properties do not directly translate to a complex cellular environment. To overcome this, multiple variants were expressed on the outer plasma membrane in cultured rat neurons and screened for brightness, photostability, membrane trafficking, and glutamate response to electrode-stimulated action potentials (Figure 2c). These efforts resulted in the iGluSnFR3.v82 and iGluSnFR3.v857 variants with 13 and 18 accumulated mutations, respectively. The latter enabled imaging of synaptic glutamate activity with improved SNR and kinetics in the mouse visual cortex.

Furthermore, biosensors can also be engineered for applications utilizing specific instrumentation. To this end, Koveal et al. coupled two-photon fluorescence lifetime imaging (2pFLIM) with microfluidics to develop a high-throughput screening system named Beadscan [42]. In this setup, single copies of library DNA are encapsulated into semipermeable gel-shell beads, in which proteins can be expressed using *in vitro* transcription/translation. The gel-shell beads are immobilized onto a glass coverslip and placed into a perfusion chamber for screening with an automated 2pFLIM microscope. The semipermeability of the beads allows for rapid exchange of buffer conditions to

screen fluorescence lifetime responses across multiple parameters and even generate dose-response curves. This allowed for the screening of a large library (>49,000 variants) and sampling of different linker lengths and compositions connecting the mTurquoise2 and lactate recognition TlpC domain resulting in the pH-insensitive lactate biosensor LiLac. Surprisingly, the *in vitro* photophysical properties as measured by BeadScan were matched to the in-cell calibration of LiLac.

Imaging Applications

Subcellular Targeting

To uncover and probe anion biology in subcellular spaces, biosensors can be fused to organelle-specific signal peptides/proteins or even proteins of interest [52]. To this end, we can look to lactate biosensors. Imaging experiments of endoplasmic reticulum (ER) targeted CanlonicSF in COS7 and HEK293 cells revealed a new contribution for the monocarboxylate transporter in ER lactate dynamics [43]. Furthermore, the excitation ratiometric feature of FiLa was used to quantitate lactate in the extracellular space, cytosol, nucleus, and mitochondria of HEK293, H1299, and HeLa cells, revealing enrichment in the latter organelle [45]. Profiling of these lactate pools with pharmacological agents provided strong evidence that lactate could be shuttled between organelles, thus acting as a signaling anion (Figure 1b).

While targeting is a useful strategy, the microenvironment of an organelle is an additional factor that must be considered for optimal in-cell performance. One noteworthy feature of the aforementioned FiLa is that it did not require calcium for lactate sensing [45]. This allowed for the quantitation of lactate in the cytosol and nucleus where calcium levels are low. Another example is the SuperFolder-LSSm-ClopHensor for simultaneous quantitation of pH and chloride in the ER [61]. The chloride-sensitive E^2GFP domain in the parent LSSm-ClopHensor was fluorescent in the cytosol, but it was non-fluorescent in the ER, due to the formation of disulfide-bridged oligomers [62]. However, this was overcome by replacing E^2GFP with the chloride-sensitive SuperFolder GFP T203Y mutant that tolerated the oxidizing environment of the ER.

At times, recognition domains in extrinsic biosensors can also induce off-target effects when overexpressed in an organelle. As one example on the cellular level, we can look to the monitoring of GTP:GDP ratios using GRISerHR in the nucleus, mitochondrial matrix, and cytosol of HEK293T cells [63]. Since the GTPase eIF5B from *Chaetomium thermophilum* was selected for GTP recognition, the enzymatic activity was eliminated to avoid depletion of the endogenous GTP reservoirs. Such interferences must also be accounted for at the organismal level as illustrated in the model plant *Arabidopsis thaliana*. For instance, the design of the sCiNiS nitrate biosensor used the nitrate-responsive transcription factor NLP7 [64]. However, this is endogenously expressed and retained in the nucleus in the presence of nitrate. To maintain this naturally occurring process, the predicted nuclear localization sequence of the NLP7 domain was mutated in sCiNiS, preventing nuclear import of the biosensor, and enabling cytosolic nitrate imaging. Additionally, when the FLIPE glutamate biosensor was expressed and displayed on the extracellular face of the plasma membrane, the transgenic plants exhibited stunted growth due to reduced glutamate signaling from competitive binding [65]. In contrast, the transgenic plants experienced wild-type growth when the biosensor was only expressed in the cytosol (Figure 3a).

Multiplex Imaging

Expanding the color palette of anion-sensitive FP biosensors is key to enable multiplex imaging. Along these lines, to generate a red-shifted biosensor for multicolor imaging of uridine diphosphate *N*-acetylglucosamine (UDP-GlcNAc) between the cytosol, ER, and Golgi apparatus, Zhang et al. first engineered the reporter domain cpmApple to improve its brightness resulting in ecpApple [66]. To recognize UDP-GlcNAc, two lectin peptides were inserted into the β-bulge of ecpApple, and further supported by a nearby non-canonical amino acid p-boronophenylalanine in the FP, resulting in bapaUGAc. As a proof of concept, bapaUGAc was targeted to the ER and paired with the green UDP-GlcNAc biosensor UGAcS in the cytosol of HEK293T cells [66,67]. Dual-color imaging with both biosensors showed the conversion of exogenously supplemented glucosamine (GlcN) to UDP-GlcNAc in the cytosol and eventual transport to the ER (Figure 3b).

The cellular dynamics of multiple analytes can also be captured with multiplex imaging. For example, glutamate is a key excitatory neurotransmitter that is coupled to calcium transients in sinoatrial node pacemaker cells (SANPCs) [68]. To visualize this, SANPCs expressing the well-established iGluSnFr on the cytosolic face of the plasma membrane were stained with the red calcium dye Cal-590 (Figure 3c) [68]. Glutamate accumulation in the cytosol correlated to local calcium release (LCR). This was stimulated by the import of glutamate into mitochondria through the excitatory amino acid transporter 1 (EAAT1) and production of reactive oxygen species, which oxidized calcium handling proteins. Imaging EAAT1 knockout cells inhibited the LCR.

Moreover, biosensors can reveal the interplay between different cell types as exemplified by $GRAB_{ATP1.0}$ expressed in the visual cortex of zebrafish larvae (Figure 3d) [69]. Using laser ablation, a local inflammatory response was triggered in the brain. As a result, ATP release occurred near this site and propagated in a distinct spatial and temporal radial fashion. At the same time, microglia expressing DsRed were activated by the inflammatory response and migrated to the site of injury along the path of ATP propagation.

2P Imaging

Imaging of opaque samples requires biosensors with near-infrared excitation and emission profiles [70]. However, given limited development in this area, biosensors with visible excitation and emission profiles are being repurposed and adapted for applications with 2P microscopy [71]. This technique relies on infrared wavelengths, which afford deeper tissue penetration with reduced light scattering and phototoxicity [72].

Motivated by the goal of *in vivo* cAMP imaging, Massengill et al. engineered the mTurquoise2-td-cp173Venus FRET-based cAMPFIRE biosensor palette [73]. The performance was validated using a 2pFLIM setup in CA1 neurons from hippocampal slices stimulated with physiologically relevant concentrations of neuromodulators. This revealed that cAMPFIRE-L had an improved affinity and dynamic range to endogenously produced cAMP. Given this, it was applied for *in vivo* imaging of layer 2/3 neurons in the

cortex. The fluorescence lifetime was measured in mice that were awake, under light anesthesia, or during locomotion (Figure 3e). In the awake state, the soma of the neurons had a lower lifetime than that observed in the dendrites within the same cell, indicating that endogenous cAMP levels were regulated with spatial selectivity. In anesthetized mice, the fluorescence lifetime decreased, stemming from lower norepinephrine and consequently cAMP levels. During locomotion, cAMP levels were dynamic showing variation between cells for the first time.

The true test of a biosensor lies in the hands of a new end user who seeks to apply an established biosensor in previously unexplored contexts [68, 74–76]. This was demonstrated by Herstel et al. with SuperClomeleon, a Cerulean-Topaz FRET biosensor from 2013 [77,78]. A new mouse model, SClm, was generated to quantitate chloride in neuronal development with 2P microscopy. In isolated hippocampal slices, chloride levels decreased in CA1 neurons as a function of culturing days *in vitro* (DIV). However, layer 2/3 neurons from the cortex at a similar age to DIV2–3 CA1 neurons, had elevated chloride levels. Thus, suggesting that the cortex matures at a later stage. It is important to note that these profound conclusions between brain regions were not made without appropriate controls and rigor. As a cautionary tale to end users, the authors disclosed the challenges with translating the FRET ratios to absolute chloride concentrations. This arose from differences in calibrating and analyzing tissues versus dissociated cell cultures. Therefore, perforated patch clamp was used as a supplement for calibrating the FRET ratios.

Summary and Outlook

Investigating anion networks across time and space dimensions at subcellular, cellular, and organismal scales is a complex feat. Here, we have highlighted how genetically encoded fluorescent biosensors can be leveraged to accelerate discovery within anion biology. While the firsts of such technologies were reported more than 20 years ago for chloride and cAMP, the recent boom points to a new dawn with challenges that remain to be addressed and boundless opportunities to do so.

From our perspective, monitoring and measuring anions necessitates a biosensor with appropriate affinity and selectivity, amongst other features, that can intercept but not interfere with a bioavailable pool. On both fronts, variability within and across biological populations or types is an inherent factor that must be accounted for when drawing conclusions. This can be resolved with a negative control or ratiometric biosensor, and even in combination with a stably expressing biological model. On a practical level, this is easier said than done, particularly when measuring. Standardized in-cell or *in vivo* calibration methods that account for confounding effects (e.g., membrane permeability, pH) are needed. If available, off-the-shelf ionophores or surfactants are commonly used, but designer technologies to directly manipulate anions are on the horizon [79–82].

In this Review, biologically relevant anions have been defined as discrete molecular species. However, this definition can be expanded to include nucleic acids, the anionic polymers of life, and even xenobiotic anions like per- and polyfluoroalkyl substances, for which biosensors already exist [83,84]. Given the modularity of the extrinsic biosensor design, it will come as no surprise when a biosensor for virtually every anion becomes available. Moreover, it is foreseeable that current trends in chemigenetic and bioluminescent biosensor designs and machine learning-guided engineering will also be adopted [85–87]. While not explicitly discussed, rigorous *in vitro* photophysical characterization and *in silico* methods can provide deep mechanistic insights [29,88]. These essential steps should not be ignored in biosensor development. Advances across all these fronts, in combination with the future development of imaging hardware and analysis software, will unlock unprecedented biological discoveries [89]. Looking beyond microscopy, new avenues will be within reach for high-throughput screening, diagnostics, and even field testing [45,90,91].

In closing, as toolmakers and end users, we believe that biosensor design and engineering can provide answers to biological questions, and vice versa. However, a single biosensor will not be the ‘champion’. In unexplored contexts, biosensor properties can be enabling or limiting, and toolmakers cannot foreshadow all possible outcomes. To the best of their ability, they should strive to be rigorous and transparent in reporting

experimental work with appropriate controls, while also open in sharing and collaborating with new end users. With these considerations, both groups can light the way forward together, illuminating anions across all forms of life and beyond.

Acknowledgements. We thank members of the Dodani Lab for valuable input during the preparation of this review. J.N.T. is an Irving S. Sigal Postdoctoral Fellow supported by the American Chemical Society. S.C.D. acknowledges support from the National Institute of General Medical Sciences of the National Institutes of Health (R35GM128923), National Science Foundation (2240095), and Welch Foundation (AT-2060-20210327). This review is the sole responsibility of the authors and does not represent the views of the funding agencies.

Figure Captions

Figure 1. The uptake, storage, and metabolism of anions is essential to all living systems. (a) Halides and oxyanions (green) are nutrients, signaling molecules, and regulators of homeostatic functions such as electrolyte balance and post-translational modifications. The carboxylates (blue) are metabolic and biosynthetic precursors serving as energy reservoirs, signaling anions, and potential biomarkers of disease states. The nucleotides (red) exist in an intricate balance, and are key energy storage molecules, secondary messengers for signal transduction, biosynthesis, and indicators of the metabolic state of the cell. Genetically encoded fluorescent biosensors can intercept and illuminate anions across these processes at the subcellular, cellular, and organismal scales. Representative biosensors discussed in this review are listed. (b) Overall β-barrel structure of avGFP from the jellyfish *Aequorea victoria* (PDB ID: 1GFL, [92]) with the chromophore equilibrium. (c) Common biosensor designs and sensing mechanisms for intrinsic and extrinsic biosensors.

Table 1. Summary of select FP biosensors for anions that were developed and/or applied from March 2021–March 2024.

Figure 2. Representative strategies used to engineer FP biosensors for anions. (a) Iterative rounds of directed evolution guided by coevolutionary modeling generates GR2-CFP. (b) Structure-guided selection and engineering of the non-coordinating residues K143 and R195 in mNeonGreen (PDB IDs: 5LTP, 5LTR, [53]) unlocked chloride sensitivity at physiological pH. Abbreviations: CRO, chromophore. (c) Improved iGluSnFR variants for *in vivo* brain imaging were generated through screening and selection in *E. coli* lysate, followed by primary rat neurons. (d) The BeadScan system to discover LiLac for 2pFLIM allowed for multi-parameter screening of individual library variants encapsulated in gel-shell beads.

Figure 3. Representative applications of FP biosensors for subcellular, multiplex, and 2P imaging of anions. (a) Localization of the FLIPE glutamate (Glu) sensor to the cytosol or plasma membrane of *A. thaliana* impacted plant growth. (b) Cytosolic localization of UGAcS and endoplasmic reticulum localization of bapaUGAC enabled UDP-GlcNAc imaging in HEK293T cells. (c) Multiplex imaging of glutamate with iGluSnFR and calcium (Ca^{2+}) with Cal-590 in sinoatrial node pacemaker cardiac cells. (d) Laser-induced injury (inset) to neurons in the visual cortex of zebrafish larvae triggered ATP release as visualized by $GRAB_{ATP1.0}$, and recruitment of DsRed-labeled astrocytes. (e) cAMPFIRE-L expressed in neurons in the somatosensory cortex of mice that were awake, anesthetized, or during locomotion revealed distinct cAMP dynamics. (f) Expression of SCIm in neurons from mice indicated intracellular chloride (Cl^-) changes in neuronal development. Abbreviations: GlcN, glucosamine, ROS, reactive oxygen species.

References

1. Frausto da Silva JRR, Williams RJP: *The Biological Chemistry of the Elements: The Inorganic Chemistry of Life*. OUP Oxford; 2001.

2. Valdivieso ÁG, Santa-Coloma TA: **The chloride anion as a signalling effector**. *Biol Rev* 2019, **94**:1839–1856.

3. Berend K, Van Hulsteijn LH, Gans ROB: **Chloride: the queen of electrolytes?** *Eur J Intern Med* 2012, **23**:203–211.

4. Li X, Yang Y, Zhang B, Lin X, Fu X, An Y, Zou Y, Wang J-X, Wang Z, Yu T: **Lactate metabolism in human health and disease**. *Sig Transduct Target Ther* 2022, **7**:1–22.

5. Featherstone DE: **Intercellular glutamate signaling in the nervous system and beyond**. *ACS Chem Neurosci* 2009, **1**:4–12.

6. Liao H-S, Chung Y-H, Hsieh M-H: **Glutamate: A multifunctional amino acid in plants**. *Plant Sci* 2022, **318**:111238.

7. Greiner JV, Glonek T: **Intracellular ATP concentration and implication for cellular evolution**. *Biology (Basel)* 2021, **10**:1166.

8. Traut TW: **Physiological concentrations of purines and pyrimidines**. *Mol Cell Biochem* 1994, **140**:1–22.

9. Cooper DMF, Tabbasum V: **Adenylate cyclase-centred microdomains**. *Biochem J* 2014, **462**:199–213.

10. Vidal EA, Alvarez JM, Araus V, Riveras E, Brooks MD, Krouk G, Ruffel S, Lejay L, Crawford NM, Coruzzi GM, et al.: **Nitrate in 2020: Thirty years from transport to signaling networks**. *Plant Cell* 2020, **32**:2094–2119.

11. Mohapatra NK, Cheng PW, Parker JC, Paradiso AM, Yankaskas JR, Boucher RC, Boat TF: **Sulfate concentrations and transport in human bronchial epithelial cells**. *Am J Physiol* 1993, **264**:C1231–1237.

12. Krasteva PV, Giglio KM, Sondermann H: **Sensing the messenger: The diverse ways that bacteria signal through c-di-GMP**. *Protein Sci* 2012, **21**:929–948.

13. Lucas KA, Pitari GM, Kazerounian S, Ruiz-Stewart I, Park J, Schulz S, Chepenik KP, Waldman SA: **Guanylyl cyclases and signaling by cyclic GMP**. *Pharmacol Rev* 2000, **52**:375–414.

14. Sunden M, Upadhyay D, Banerjee R, Sipari N, Fellman V, Kallijärvi J, Purhonen J: **Enzymatic assay for UDP-GlcNAc and its application in the parallel**

assessment of substrate availability and protein O-GlcNAcylation. *Cell Rep Methods* 2023, **3**:100518.

15. Lee T-Y: **Lactate: a multifunctional signaling molecule**. *Yeungnam Univ J Med* 2021, **38**:183–193.

16. Pang K, Wang W, Qin J, Shi Z, Hao L, Ma Y, Xu H, Wu Z, Pan D, Chen Z, et al.: **Role of protein phosphorylation in cell signaling, disease, and the intervention therapy**. *MedComm (2020)* 2022, **3**:e175.

17. Alnouti Y: **Bile Acid sulfation: a pathway of bile acid elimination and detoxification**. *Toxicol Sci* 2009, **108**:225–246.

18. Ashton TD, Jolliffe KA, Pfeffer FM: **Luminescent probes for the bioimaging of small anionic species in vitro and in vivo**. *Chem Soc Rev* 2015, **44**:4547–4595.

19. Kovermann P, Engels M, Müller F, Fahlke C: **Cellular physiology and pathophysiology of EAAT anion channels**. *Front Cell Neurosci* 2022, **15**:815279.

20. Wardak C, Morawska K, Pietrzak K: **New materials used for the development of anion-selective electrodes—A review**. *Materials (Basel)* 2023, **16**:5779.

21. Tsien RY: **The green fluorescent protein**. *Annu Rev Biochem* 1998, **67**:509–544.

22. Greenwald EC, Mehta S, Zhang J: **Genetically encoded fluorescent biosensors illuminate the spatiotemporal regulation of signaling networks**. *Chem Rev* 2018, **118**:11707–11794.

23. Palmer AE, Qin Y, Park JG, McCombs JE: **Design and application of genetically encoded biosensors**. *Trends in Biotechnol* 2011, **29**:144–152.

24. Wachter RM, Remington SJ: **Sensitivity of the yellow variant of green fluorescent protein to halides and nitrate**. *Curr Biol* 1999, **9**: R628–R629.

25. Arosio D, Garau G, Ricci F, Marchetti L, Bizzarri R, Nifosì R, Beltram F: **Spectroscopic and structural study of proton and halide ion cooperative binding to GFP**. *Biophys J* 2007, **93**:232–244.

26. Lodovichi C, Ratto GM, Trevelyan AJ, Arosio D: **Genetically encoded sensors for Chloride concentration**. *J Neurosci Methods* 2022, **368**:109455.

27. Salto R, Giron MD, Puente-Muñoz V, Vilchez JD, Espinar-Barranco L, Valverde-Pozo J, Arosio D, Paredes JM: **New red-emitting chloride-sensitive fluorescent protein with biological uses**. *ACS Sens* 2021, **6**:2563–2573.

28. Peng W, Maydew CC, Kam H, Lynd JK, Tutol JN, Phelps SM, Abeyrathna S, Meloni G, Dodani SC: **Discovery of a monomeric green fluorescent protein sensor for**

chloride by structure-guided bioinformatics. *Chemical Science* 2022, **13**:12659–12672.

29. Ong WSY, Ji K, Pathiranage V, Maydew C, Baek K, Villones RLE, Meloni G, Walker AR, Dodani SC: **Rational design of the β-bulge gate in a green fluorescent protein accelerates the kinetics of sulfate sensing**. *Angew Chemie Int Ed Engl* 2023, **62**:e202302304.

30. Tutol JN, Ong WSY, Phelps SM, Peng W, Goenawan H, Dodani SC: **Engineering the ChlorON series: Turn-on fluorescent protein sensors for imaging labile chloride in living cells**. *ACS Cent Sci* 2024, **10**:77–86.

31. Tutol JN, Lee J, Chi H, Faizuddin FN, Abeyrathna SS, Zhou Q, Morcos F, Meloni G, Dodani SC: **A single point mutation converts a proton-pumping rhodopsin into a red-shifted, turn-on fluorescent sensor for chloride**. *Chem Sci* 2021, **12**:5655–5663.

32. Chi H, Zhou Q, Tutol JN, Phelps SM, Lee J, Kapadia P, Morcos F, Dodani SC: **Coupling a live cell directed evolution assay with coevolutionary landscapes to engineer an improved fluorescent rhodopsin chloride sensor**. *ACS Synth Biol* 2022, **11**:1627–1638.

33. Phelps SM, Tutol JN, Advani D, Peng W, Dodani SC: **Unlocking chloride sensing in the red at physiological pH with a fluorescent rhodopsin-based host**. *Chem Commun* 2023, **59**:8460–8463.

34. Baird GS, Zacharias DA, Tsien RY: **Circular permutation and receptor insertion within green fluorescent proteins**. *PNAS* 1999, **96**:11241–11246.

35. Nasu Y, Shen Y, Kramer L, Campbell RE: **Structure- and mechanism-guided design of single fluorescent protein-based biosensors**. *Nat Chem Biol* 2021, **17**:509–518.

36. Sanchez C, Ramirez A, Hodgson L: **Unravelling molecular dynamics in living cells: Fluorescent protein biosensors for cell biology**. *J Microsc* 2024, DOI: 10.1111/jmi.13270.

37. Bekdash R, Quejada JR, Ueno S, Kawano F, Morikawa K, Klein AD, Matsumoto K, Lee TC, Nakanishi K, Chalan A, et al.: **GEM-IL: A highly responsive fluorescent lactate indicator**. *Cell Rep Methods* 2021, **1**:100092.

38. Nasu Y, Murphy-Royal C, Wen Y, Haidey JN, Molina RS, Aggarwal A, Zhang S, Kamijo Y, Paquet M-E, Podgorski K, et al.: **A genetically encoded fluorescent biosensor for extracellular L-lactate**. *Nat Commun* 2021, **12**:7058.

39. Nasu Y, Aggarwal A, Le GNT, Vo CT, Kambe Y, Wang X, Beinlich FRM, Lee AB, Ram TR, Wang F, et al.: **Lactate biosensors for spectrally and spatially multiplexed fluorescence imaging**. *Nat Commun* 2023, **14**:6598.

40. Hario S, Le GNT, Sugimoto H, Takahashi-Yamashiro K, Nishinami S, Toda H, Li S, Marvin JS, Kuroda S, Drobizhev M, et al.: **High-performance genetically encoded green fluorescent biosensors for intracellular L-lactate**. *ACS Cent Sci* 2024, **10**:402–416.

41. Wellbourne-Wood J, Briquet M, Alessandri M, Binda F, Touya M, Chatton J-Y: **Evaluation of hydroxycarboxylic acid receptor 1 (HCAR1) as a building block for genetically encoded extracellular lactate biosensors**. *Biosensors* 2022, **12**:143.

42. Koveal D, Rosen PC, Meyer DJ, Díaz-García CM, Wang Y, Cai LH, Chou PJ, Weitz DA, Yellen G: **A high-throughput multiparameter screen for accelerated development and optimization of soluble genetically encoded fluorescent biosensors**. *Nat Commun* 2022, **13**:2919.

43. Aburto C, Galaz A, Bernier A, Sandoval PY, Holtheuer-Gallardo S, Ruminot I, Soto-Ojeda I, Hertenstein H, Schweizer JA, Schirmeier S, et al.: **Single-fluorophore indicator to explore cellular and sub-cellular lactate dynamics**. *ACS Sens* 2022, **7**:3278–3286.

44. Xu X, Xu R, Hou S, Kang Z, Lü C, Wang Q, Zhang W, Wang X, Xu P, Gao C, et al.: **A selective fluorescent L-lactate biosensor based on an L-lactate-specific transcription regulator and Förster resonance energy transfer**. *Biosensors* 2022, **12**:1111.

45. Li X, Zhang Y, Xu L, Wang A, Zou Y, Li T, Huang L, Chen W, Liu S, Jiang K, et al.: **Ultrasensitive sensors reveal the spatiotemporal landscape of lactate metabolism in physiology and disease**. *Cell Metab* 2023, **35**:200–211.e9.

46. Wang Y, Xue P, Cao M, Yu T, Lane ST, Zhao H: **Directed evolution: Methodologies and applications**. *Chem Rev* 2021, **121**:12384–12444.

47. McLure RJ, Radford SE, Brockwell DJ: **High-throughput directed evolution: a golden era for protein science**. *Trends Chem* 2022, **4**:378–391.

48. Yang J, Zhang Y: **I-TASSER server: new development for protein structure and function predictions**. *Nucleic Acids Res* 2015, **43**:W174–W181.

49. Waterhouse A, Bertoni M, Bienert S, Studer G, Tauriello G, Gumienny R, Heer FT, de Beer TAP, Rempfer C, Bordoli L, et al.: **SWISS-MODEL: homology modelling of protein structures and complexes**. *Nucleic Acids Res* 2018, **46**:W296–W303.

50. Morcos F, Pagnani A, Lunt B, Bertolino A, Marks DS, Sander C, Zecchina R, Onuchic JN, Hwa T, Weigt M: **Direct-coupling analysis of residue coevolution captures native contacts across many protein families**. *PNAS* 2011, **108**:E1293–E1301.

51. Tutol JN, Kam HC, Dodani SC: **Identification of mNeonGreen as a pH-Dependent, Turn-On Fluorescent Protein Sensor for Chloride**. *ChemBioChem* 2019, **20**:1759–1765.

52. Shaner NC, Lambert GG, Chammas A, Ni Y, Cranfill PJ, Baird MA, Sell BR, Allen JR, Day RN, Israelsson M, et al.: **A bright monomeric green fluorescent protein derived from Branchiostoma lanceolatum**. *Nature Methods* 2013, **10**:407–409.

53. Clavel D, Gotthard G, von Stetten D, De Sanctis D, Pasquier H, Lambert GG, Shaner NC, Royant A: **Structural analysis of the bright monomeric yellow-green fluorescent protein mNeonGreen obtained by directed evolution**. *Acta Crystallogr D Struct Biol* 2016, **72**:1298–1307.

54. Chen Z, Zhao H: **Rapid creation of a novel protein function by in vitro coevolution**. *J Mol Biol* 2005, **348**:1273–1282.

55. Marcus Y: **A simple empirical model describing the thermodynamics of hydration of ions of widely varying charges, sizes, and shapes**. *Biophys Chem* 1994, **51**:111–127.

56. Davidsen K, Marvin JS, Aggarwal A, Brown TA, Sullivan LB: **An engineered biosensor enables dynamic aspartate measurements in living cells**. *eLife* 2024, **12**:RP90024.

57. Schmidt-Dannert C, Arnold FH: **Directed evolution of industrial enzymes**. *Trends Biotechnol* 1999, **17**:135–136.

58. Hendel SJ, Shoulders MD: **Directed evolution in mammalian cells**. *Nat Methods* 2021, **18**:346–357.

59. Aggarwal A, Liu R, Chen Y, Ralowicz AJ, Bergerson SJ, Tomaska F, Mohar B, Hanson TL, Hasseman JP, Reep D, et al.: **Glutamate indicators with improved activation kinetics and localization for imaging synaptic transmission**. *Nat Methods* 2023, **20**:925–934.

60. Hao Y, Plested AJR: **Seeing glutamate at central synapses**. *J Neurosci Methods* 2022, **375**:109531.

61. Shariati K, Zhang Y, Giubbolini S, Parra R, Liang S, Edwards A, Hejtmancik JF, Ratto GM, Arosio D, Ku G: **A superfolder green fluorescent protein-based biosensor allows monitoring of chloride in the endoplasmic reticulum**. *ACS Sens* 2022, **7**:2218–2224.

62. Paredes JM, Idilli AI, Mariotti L, Losi G, Arslanbaeva LR, Sato SS, Artoni P, Szczurkowska J, Cancedda L, Ratto GM, et al.: **Synchronous bioimaging of intracellular pH and chloride based on LSS fluorescent protein**. *ACS Chem Biol* 2016, **11**:1652–1660.

63. Zhang M, Yang B, Zhang J, Song Y, Wang W, Li N, Wang Y, Li W, Wang J: **Monitoring the dynamic regulation of the mitochondrial GTP-to-GDP ratio with a genetically encoded fluorescent biosensor**. *Angew Chemie Int Ed* 2022, **61**:e202201266.

64. Liu K-H, Liu M, Lin Z, Wang Z-F, Chen B, Liu C, Guo A, Konishi M, Yanagisawa S, Wagner G, et al.: **NIN-like protein 7 transcription factor is a plant nitrate sensor**. *Science* 2022, **377**:1419–1425.

65. Castro-Rodríguez V, Kleist TJ, Gappel NM, Atanjaoui F, Okumoto S, Machado M, Denyer T, Timmermans MCP, Frommer WB, Wudick MM: **Sponging of glutamate at the outer plasma membrane surface reveals roles for glutamate in development**. *Plant J* 2022, **109**:664–674.

66. Zhang J, Li Z, Pang Y, Fan Y, Ai H: **Genetically encoded boronolectin as a specific red fluorescent UDP-GlcNAc biosensor**. *ACS Sens* 2023, **8**:2996–3003.

67. Li Z, Zhang J, Ai H: **Genetically encoded green fluorescent biosensors for monitoring UDP-GlcNAc in live cells**. *ACS Cent Sci* 2021, **7**:1763–1770.

68. Xie D, Xiong K, Su X, Wang G, Zou Q, Wang L, Zhang C, Cao Y, Shao B, Zhang Y, et al.: **Glutamate drives 'local Ca2+ release' in cardiac pacemaker cells**. *Cell Res* 2022, **32**:843–854.

69. Wu Z, He K, Chen Y, Li H, Pan S, Li B, Liu T, Xi F, Deng F, Wang H, et al.: **A sensitive GRAB sensor for detecting extracellular ATP in vitro and in vivo**. *Neuron* 2022, **110**:770–782.e5.

70. Shcherbakova DM, Stepanenko OV, Turoverov KK, Verkhusha VV: **Near-infrared fluorescent proteins: multiplexing and optogenetics across scales**. *Trends Biotechnol* 2018, **36**:1230–1243.

71. Yellen G, Mongeon R: **Quantitative two-photon imaging of fluorescent biosensors**. *Curr Opin Chem Biol* 2015, **27**:24–30.

72. Benninger RKP, Piston DW: **Two-photon excitation microscopy for the study of living cells and tissues**. *Curr Protoc Cell Biol* 2013, **4**:4.11.1–4.11.24.

73. Massengill CI, Bayless-Edwards L, Ceballos CC, Cebul ER, Cahill J, Bharadwaj A, Wilson E, Qin M, Whorton MR, Baconguis I, et al.: **Sensitive genetically encoded sensors for population and subcellular imaging of cAMP in vivo**. *Nat Methods* 2022, **19**:1461–1471.

74. Rahmati N, Normoyle KP, Glykys J, Dzhala VI, Lillis KP, Kahle KT, Raiyyani R, Jacob T, Staley KJ: **Unique actions of GABA arising from cytoplasmic chloride microdomains**. *J Neurosci* 2021, **41**:4957–4975.

75. Jiménez-Gómez B, Ortega-Sáenz P, Gao L, González-Rodríguez P, García-Flores P, Chandel N, López-Barneo J: **Transgenic NADH dehydrogenase restores oxygen regulation of breathing in mitochondrial complex I-deficient mice**. *Nat Commun* 2023, **14**:1172.

76. Peng Q, Bao W, Geng B, Yang S: **Biosensor-assisted CRISPRi high-throughput screening to identify genetic targets in Zymomonas mobilis for high d-lactate production**. *Synth Syst Biotechnol* 2024, **9**:242–249.

77. Grimley JS, Li L, Wang W, Wen L, Beese LS, Hellinga HW, Augustine GJ: **Visualization of synaptic inhibition with an optogenetic sensor developed by cell-free protein engineering automation**. *J Neurosci* 2013, **33**:16297–16309.

78. Herstel LJ, Peerboom C, Uijtewaal S, Selemangel D, Karst H, Wierenga CJ: **Using SuperClomeleon to measure changes in intracellular chloride during development and after early life stress**. *eNeuro* 2022, **9**:ENEURO.0416–22.2022.

79. Jayaraman S, Haggie P, Wachter R M, Remington S J, Verkman A S: **Mechanism and cellular applications of a green fluorescent protein-based halide sensor**. *J Biol Chem* 2000, **275**:6047–6050.

80. Zhao Y, Shen Y, Wen Y, Campbell R E: **High-performance intensiometric direct- and inverse-response genetically encoded biosensors for citrate**. *ACS Cent Sci* 2020, **6**: 1441–1450.

81. Ryder W G, Graziotto M E, Levina A, Hawkins B, Hibbs D E, New E J, Gale P A. **Subcellular targeted anion transporters**. *ChemRxiv* Preprint 2024, DOI: 10.26434/chemrxiv-2023-m3p3j-v2.

82. Miyazaki I, Tsao K K, Kamijo Y, Nasu Y, Terai T, Campbell R E: **Synthesis and application of a photocaged L-lactate.** *bioRxiv* Preprint 2024, DOI: 10.1101/2024.01.30.577898v1.

83. Braselmann E, Rathbun C, Richards E M, Palmer A E: **Illuminating RNA Biology: Tools for Imaging RNA in Live Mammalian Cells**. *Cell Chem Biol* 2020, **27**: 891–903.

84. Mann M M, Berger, B W: **A genetically-encoded biosensor for direct detection of perfluorooctanoic acid**. *Sci Rep* 2023, **13**:15186.

85. Hellweg L, Edenhofer A, Barck L, Huppertz M-C, Frei M S, Tarnawski M, Bergner A, Koch B, Johnsson K, Hiblot J: **A general method for the development of multicolor biosensors with large dynamic ranges**. *Nat Chem Biol* 2023, **19**:1147–1157.

86. Petersen E D, Lapan A P, Franco E A C, Fillion A J, Crespo E L, Lambert G G, Grady C J, Zanca A T, Orcutt R, Hochgeschwender U, et al.: B**ioluminescent**

genetically encoded glutamate indicators for molecular imaging of neuronal activity. *ACS Synth Biol* 2023, **12**:2301–2309.

87. Wait S, Expòsit M, Lin S, Rappleye M, Lee J D, Colby S A, Torp L, Asencio A, Smith A, Regnier M, et al.: **Machine learning-guided engineering of genetically encoded fluorescent calcium indicators**. *Nat Comput Sci* 2024, **4**:224–236.

88. Chen C, Tutol J N, Tang L, Zhu L, Ong W S Y, Dodani S C, Fang C: **Excitation ratiometric chloride sensing in a standalone yellow fluorescent protein is powered by the interplay between proton transfer and conformational reorganization**. *Chem Sci* 2021, **12**:11382–11393.

89. Yao Z, Brennan C K, Scipioni L, Chen H, Ng K K, Tedeschi G, Parag-Sharma K, Amelio A L, Gratton E, Digman M A, Prescher J A: **Multiplexed bioluminescence microscopy via phasor analysis**. *Nat Methods* 2022, **19**: 893–898.

90. Koh A, Kang D, Xue Y, Lee S, Pielak R M, Kim J, Hwang T, Min S, Banks A, Bastien P, et al.: **A soft, wearable microfluidic device for the capture, storage, and colorimetric sensing of sweat**. *Sci Transl Med* 2016, **8**: 366ra165.

91. Thavarajah W, Silverman A D, Verosloff M S, Kelley-Loughnane N, Jewett M C, Lucks J B: **Point-of-use detection of environmental fluoride via a cell-free riboswitch-based biosensor**. *ACS Synth Biol* 2020, **9**:10–18.

92. Yang F, Moss LG, Phillips GN: **The molecular structure of green fluorescent protein**. *Nat Biotechnol* 1996, **14**:1246–1251.

93. Pracucci E, Graham RT, Alberio L, Nardi G, Cozzolino O, Pillai V, Pasquini G, Saieva L, Walsh D, Landi S, et al.: **Daily rhythm in cortical chloride homeostasis underpins functional changes in visual cortex excitability**. *Nat Commun* 2023, **14**:7108.

94. Călin A, Waseem T, Raimondo JV, Newey SE, Akerman CJ: **A genetically targeted ion sensor reveals distinct seizure-related chloride and pH dynamics in GABAergic interneuron populations**. *iScience* 2023, **26**:106363.

95. Klett NJ, Cravetchi O, Allen NC: **Long-term imaging reveals a circadian rhythm of intracellular chloride in neurons of the suprachiasmatic nucleus**. *J Biol Rhythms* 2022, **37**:110–123.

96. Chen Y-N, Ho C-H: **Concept of fluorescent transport activity biosensor for the characterization of the Arabidopsis NPF1.3 activity of nitrate**. *Sensors (Basel)* 2022, **22**:1198.

97. Chen Y-N, Cartwright HN, Ho C-H: **In vivo visualization of nitrate dynamics using a genetically encoded fluorescent biosensor**. *Sci Adv* 2022, **8**:eabq4915.

98. Zhang S, Daniels DA, Ivanov S, Jurgensen L, Müller LM, Versaw WK, Harrison MJ: **A genetically encoded biosensor reveals spatiotemporal variation in cellular**

phosphate content in Brachypodium distachyon mycorrhizal roots. *New Phytol* 2022, **234**:1817–1831.

99. Luan M, Zhao F, Sun G, Xu M, Fu A, Lan W, Luan S: **A SPX domain vacuolar transporter links phosphate sensing to homeostasis in *Arabidopsis***. *Mol Plant* 2022, **15**:1590–1601.

100. Chen W, Natan RG, Yang Y, Chou S-W, Zhang Q, Isacoff EY, Ji N: **In vivo volumetric imaging of calcium and glutamate activity at synapses with high spatiotemporal resolution**. *Nat Commun* 2021, **12**:6630.

101. Wang CS, Chanaday NL, Monteggia LM, Kavalali ET: **Probing the segregation of evoked and spontaneous neurotransmission via photobleaching and recovery of a fluorescent glutamate sensor**. *eLife* 2022, **11**:e76008.

102. Hao Y, Toulmé E, König B, Rosenmund C, Plested AJ: **Targeted sensors for glutamatergic neurotransmission**. *eLife* 2023, **12**:e84029.

103. Hatashita Y, Wu Z, Fujita H, Kumamoto T, Livet J, Li Y, Tanifuji M, Inoue T: **Spontaneous and multifaceted ATP release from astrocytes at the scale of hundreds of synapses**. *Glia* 2023, **71**:2250–2265.

104. Tenner B, Zhang JZ, Kwon Y, Pessino V, Feng S, Huang B, Mehta S, Zhang J: **FluoSTEPs: Fluorescent biosensors for monitoring compartmentalized signaling within endogenous microdomains**. *Sci Adv* 2021, **7**:eabe4091.

105. Hardy JC, Mehta S, Zhang J: **Measuring spatiotemporal cAMP dynamics within an endogenous signaling compartment using FluoSTEP-ICUE**. *Methods Mol Biol* 2022, **2483**:351–366.

106. Wang L, Wu C, Peng W, Zhou Z, Zeng J, Li X, Yang Y, Yu S, Zou Y, Huang M, et al.: **A high-performance genetically encoded fluorescent indicator for in vivo cAMP imaging**. *Nat Commun* 2022, **13**:5363.

107. Liu W, Liu C, Ren P-G, Chu J, Wang L: **An improved genetically encoded fluorescent cAMP indicator for sensitive cAMP imaging and fast drug screening**. *Front Pharmacol* 2022, **13**:902290.

108. Kawata S, Mukai Y, Nishimura Y, Takahashi T, Saitoh N: **Green fluorescent cAMP indicator of high speed and specificity suitable for neuronal live-cell imaging**. *PNAS* 2022, **119**:e2122618119.

109. Yokoyama T, Manita S, Uwamori H, Tajiri M, Imayoshi I, Yagishita S, Murayama M, Kitamura K, Sakamoto M: **A multicolor suite for deciphering population coding of calcium and cAMP in vivo**. *Nat Methods* 2024, DOI: 10.1038/s41592-024-02222-9.

110. Pollock AJ, Choi PH, Zaver SA, Tong L, Woodward JJ: **A rationally designed c-di-AMP Förster resonance energy transfer biosensor to monitor nucleotide dynamics**. *J Bacteriol* 2021, **203**:e0008021.

111. Takizawa M, Osuga Y, Ishida R, Mita M, Harada K, Ueda H, Kitaguchi T, Tsuboi T: **Development of a red fluorescent protein-based cGMP indicator applicable for live-cell imaging**. *Commun Biol* 2022, **5**:1–9.

112. Halte M, Wörmann ME, Bogisch M, Erhardt M, Tschowri N: **BldD-based bimolecular fluorescence complementation for in vivo detection of the second messenger cyclic di-GMP**. *Mol Microbiol* 2022, **117**:705–713.

113. Ide H, Hayashida Y, Morimoto YV: **Visualization of c-di-GMP in multicellular Dictyostelium stages**. *Front Cell Dev Biol* 2023, **11**:1237778.

Figure 1

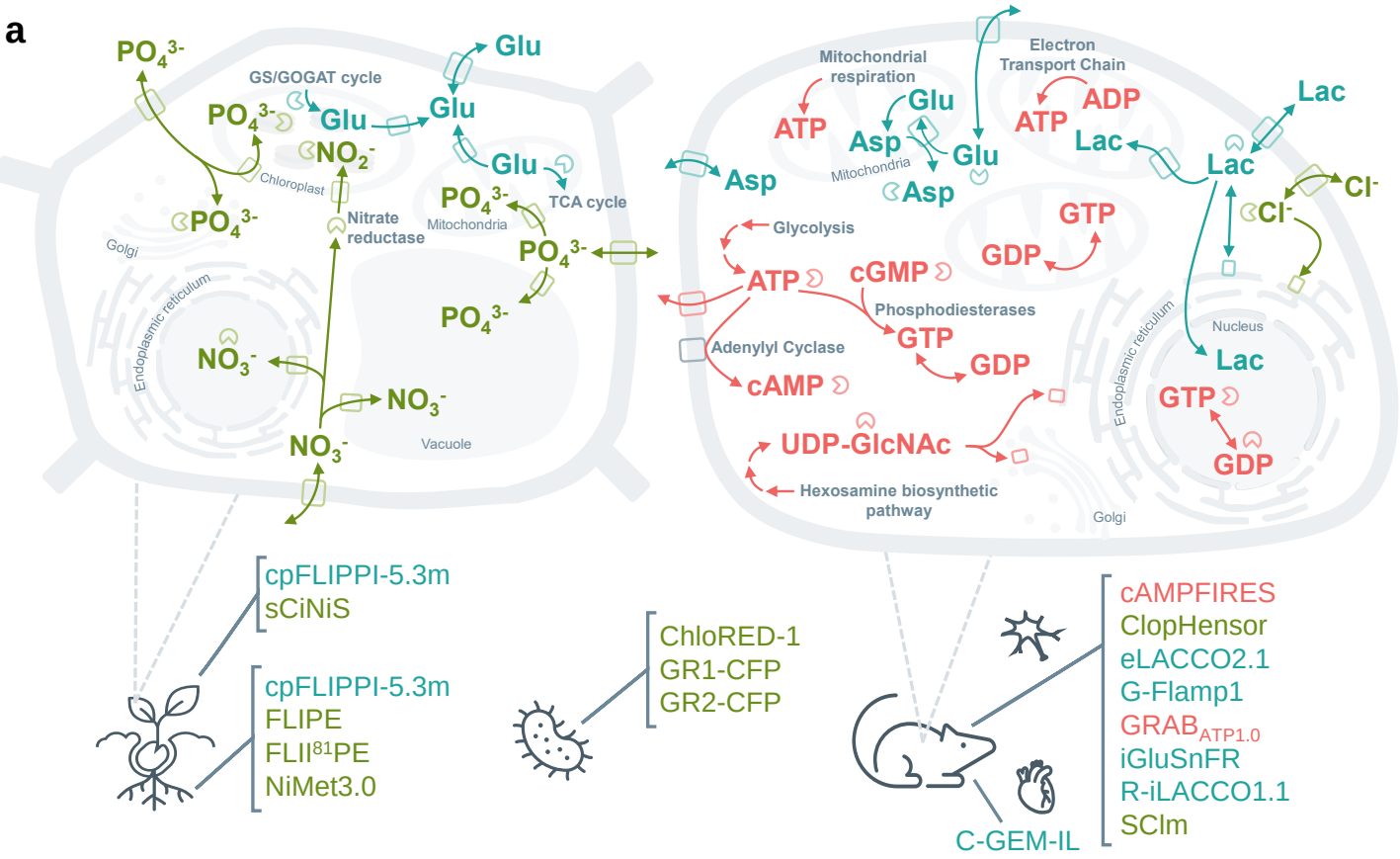

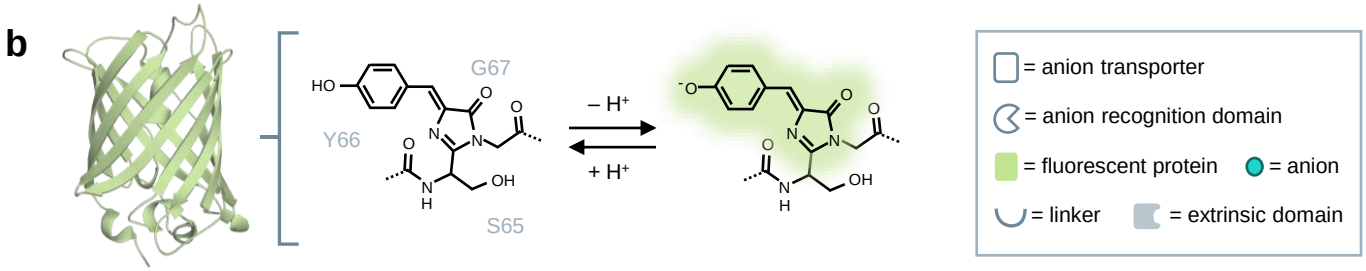

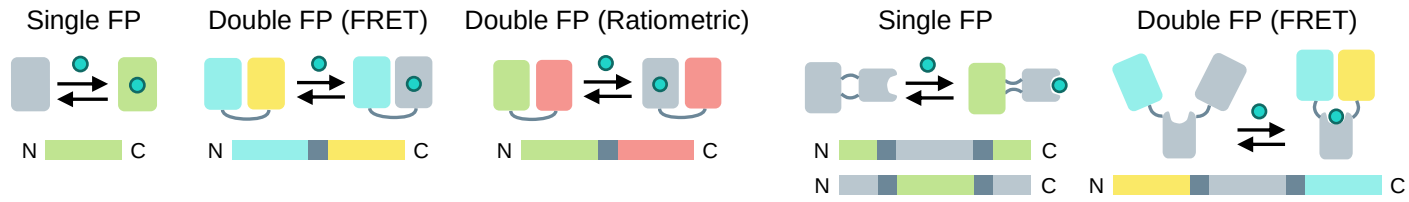

https://doi.org/10.26434/chemrxiv-2024-zvtvr-v2 **ORCID:** https://orcid.org/0000-0003-0271-6080

Table 1

Anion	Sensor Name	Output	λ_{ex} (nm) free (bound)	λ_{em} (nm) free (bound)	K_d (mM)	ε free (bound) mM^{-1} cm^{-1}	φ free (bound)	Reference(s)
Chloride	GR1-CFP	Ratiometric	390, 530	705	42	—	0.003 (0.0039)	31
	GR2-CFP	Ratiometric	390, 570	485, 705	53	—	—	32
	ChloRED-1-CFP	Ratiometric	440, 615	475, 710	23.1	—	—	33
	mBerFP S94V-R205Y	Ratiometric	380, 440	495, 610	106	11840	0.85	27
	LSSmClopHensor	Ratiometric	800, 830, 860, 910, 960	527, 607	—	—	—	93
	LSSmsfClopHensor	Ratiometric	458	—	7.9	—	—	61
	ER-LSSmClopHensor	Ratiometric	458	—	—	—	—	61
	ClopHensorN	Ratiometric	458, 488, 561	—	8.73	—	—	94
	Cl-Sensor	Ratiometric	436, 500	—	—	—	—	95
	GFPxm163	Intensiometric	480	524	230.1	67,845 (9,453)	0.89 (0.08)	28
	SuperClomelon	FRET	840	485, 535	—	—	—	78
	ChlorON-1	Intensiometric	480	515	285	27,400 (24,200)	< 0.01 (0.027)	30
	ChlorON-2	Intensiometric	480	515	55	21,900 (20,900)	< 0.01 (0.092)	30
	ChlorON-3	Intensiometric	480	515	30	15,600 (18,700)	< 0.01 (0.152)	30
Nitrate	NiTrac-NPF1.3	FRET	440, 514	488, 530	—	—	—	96
	sCiNiS	Intensiometric	—	—	0.052	—	—	64
	NiMet3.0	FRET	428	488, 530	0.09	—	—	97
Phosphate	cpFLIPPi-5.3m	FRET	—	—	—	—	—	98,99
Sulfate	SulfOFF-1	Intensiometric	485	520	0.2	94,511 (26,466)	0.69 (0.59)	29
Glutamate	iGluSnFR	Intensiometric	940	—	—	—	—	100
		Intensiometric	488	—	—	—	—	68
		FRAP	—	—	—	—	—	101
	SnFR-γ2	Intensiometric	488	—	—	—	—	102
	SnFR-γ8	Intensiometric	488	—	—	—	—	102
	iGluSnFR3v82	Intensiometric	505	525	—	—	—	59
	iGluSnFR3v857	Intensiometric	505	525	—	—	—	59
	FLIPE-600n	Intensiometric	470	525	0.0006	—	—	65
	FLII81 PE-1μ	FRET	470	495, 525	0.001	—	—	65
	FLIPE-10μ	Intensiometric	470	525	0.01	—	—	65
	FLIPE-1m	Intensiometric	470	525	1	—	—	65
Lactate	GEM-IL	Intensiometric	425	490	0.661	—	—	37

Lactate	eLACCO1.1	Intensiometric	493 (496)	510	3.9	78 (89)	0.60(0.78)	35
	eLACCO2.1	Intensiometric	492	509	0.96	76	0.17	38
	R-iLACCO1	Intensiometric	574	604	0.074	84	0.17	39
	iLACCO1	Intensiometric	492 (493)	511 (510)	0.361	—	0.72 (0.84)	40
	iLACCO1.1	Intensiometric	493 (493)	510 (510)	4.55	—	0.57 (0.57)	40
	iLACCO1.2	Intensiometric	493 (493)	510 (509)	0.0169	—	0.61 (0.86)	40
	LARS1.8	Intensiometric	488	515	1.5	—	—	41
	LARS1.10	Intensiometric	488	515	5.6	—	—	41
	LiLac	Intensiometric	438 (440)	489 (494)	2.7	31.0 (28.6)	0.87 (0.56)	42
	CanlonicSF	Intensiometric	485	530	0.293	—	—	43
	$FILLac_{10N0C}$	FRET	430	492, 526	0.00633	—	—	44
	FiLa	Excitation ratiometric	425, 490	514	0.13	425 nm 22900(15300) 490 nm 4900(23600)	425 nm 0.31(0.08) 490 nm 0.22(0.11)	45
ATP	$GRAB_{ATP1.0}$	Intensiometric	500	520	0.0067	—	—	69
		Intensiometric	488	520	—	—	—	103
cAMP	FluoSTEP-ICUE	FRET	480	563	—	—	—	104, 105
	G-Flamp1	Intensiometric	500 (490)	513 (510)	0.00217	4374 (25,280)	0.323 (0.322)	106
	G-Flamp2	Intensiometric	496 (488)	519 (516)	—	5189 (45,459)	0.38 (0.33)	107
	G-Flamp2b	Intensiometric	496 (488)	519 (516)	0.0019	12528 (33,760)	0.39 (0.37)	107
	CAMPFIRE-L	FRET	430	—	0.0027	—	—	73
	CAMPFIRE-M	FRET	430	—	0.00145	—	—	73
	CAMPFIRE-H	FRET	430	—	0.00038	—	—	73
	gCarvi	Intensiometric	485	535	1.5	14,000,000 (20,600,000)	0.53 (0.79)	108
	cAMPinG1	Excitation ratiometric	405, 488	535	—	—	—	109
c-di-AMP	CDA5	FRET	425	480, 535	—	—	—	110
GTP/GDP	GRISer	Excitation ratiometric	405, 488	—	0.07	—	—	63
	GRISerHR	Excitation ratiometric	405, 488	—	7	—	—	63
cGMP	Red cGull	Intensiometric	567	591	0.00033[a]	988,000 (5,638,000)	0.149 (0.225)	111
c-di-GMP	CensYBL	Intensiometric	510, 590	540, 620	—	—	—	112
	YFP-YcgR-CFP	FRET	430	460, 520	—	—	—	113
UDP/UTP	UXPS	Excitation ratiometric	400, 488	—	0.006	—	—	67
UDP-GlcNAc	UGAcS	Excitation ratiometric	400, 488	—	0.072	—	—	67
	bapaUGAc	Intensiometric	575	600	2.14	—	—	66

[a]EC_{50} is reported instead of K_d.

Figure 2

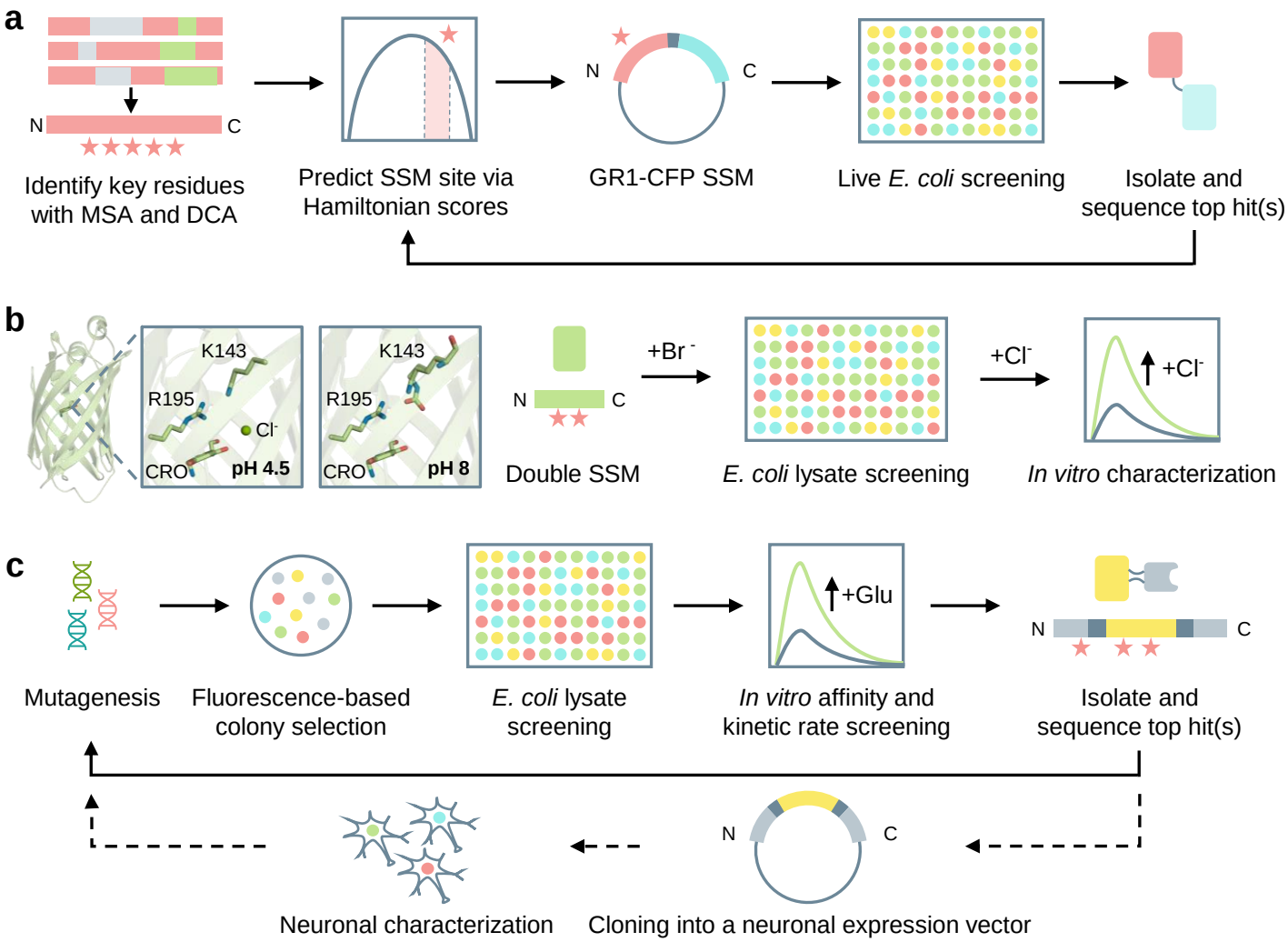

Figure 3